Transactions on Energy Systems and Engineering Applications

Article

Fuel Cell Based Ultra-Voltage Gain Boost Converter for Electric Vehicle Applications

B. Nagi Reddy[1,*], G. Vinay Kumar[1], B. Vinay Kumar[1], B. Jhansi[1], B. Sandeep[1], and K. Sarada[2]

[1] Department of Electrical and Electronics Engineering, Vignana Bharathi Institute of Technology, Hyderabad, India.
[2] Department of Electrical and Electronics Engineering, Koneru Lakshmaiah Education Foundation, Vijayawada, India.
* Correspondence: nagireddy208@gmail.com

Received: 19 May 2023; Accepted: 10 June 2023; Published: 19 June 2023

Abstract: The proposed fuel cell-based ultra-voltage gain boost converter offers an alternative to transformer-based topologies for achieving high voltage gain. While transformers can achieve high voltage gains, they come with drawbacks such as high cost, design complexity, and increased weight. In this article, a switched inductor circuit is introduced as an alternative solution to achieve high voltage gain. This circuit enhances overall system performance by reducing size, weight, and cost. Operating in a transformer-less topology, the converter boosts voltage levels while ensuring low voltage stress on the switching devices. The suggested design enables larger voltage gain values even at low duty ratios. The output of the fundamental boost converter serves as the input for the switched inductor circuit, effectively boosting the voltage level and supplying more voltage to the output side. This converter is particularly suitable for applications requiring ultra-voltage gain in electric vehicles, which offer reduced pollution compared to internal combustion engines. Moreover, the utilization of this topology reduces space requirements. The article presents a thorough investigation of the steady state operation in continuous conduction mode, and theoretical verification and MATLAB simulations demonstrate the performance and operation of the proposed converter.

1. Introduction

Present-day applications for DC-DC converters include photovoltaic energy systems, electric vehicle systems, and numerous industrial and automotive systems. Stepping up the voltage from a low level to a higher one is crucial for improving the performance of the working system such as an EV system; see Figure 1.

How to cite this article: B. Nagi Reddy, G. Vinay Kumar, B. Vinay Kumar, B. Jhansi, B. Sandeep and K. Sarada. Fuel Cell Based Ultra-Voltage Gain Boost Converter for Electric Vehicle Applications . *Transactions on Energy Systems and Engineering Applications*, 4(1): 519, 2023. DOI:10.32397/tesea.vol4.n1.519

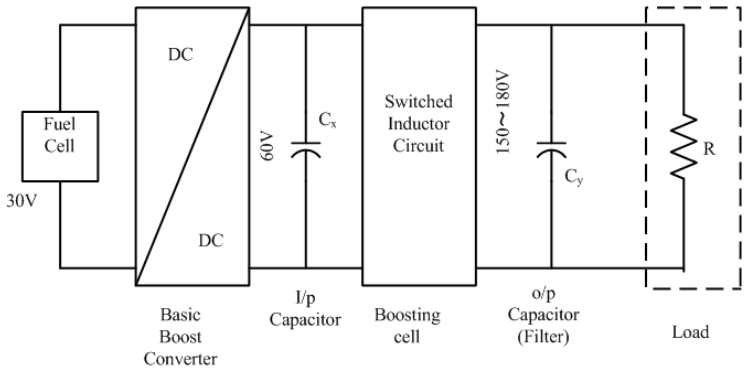

Figure 1. Fuel cell-based voltage gain dc-dc converter.

A higher output voltage is necessary for a basic EV system to generate propulsion for a vehicle. The series connection of cells or batteries will increase the output voltage. However, several hundreds of batteries are employed which might be a major challenge as the amount of space needed in the EV systems increases. The output voltage can be increased and high voltage gain achieved by using a fuel cell-based ultra-high voltage gain boost converter. This converter would make it possible to attain ultra-voltage gains with greater efficiencies under low voltage stresses while requiring less room and battery maintenance.

The output voltage of fuel cells is primarily direct current (DC) and typically exhibits variations with load. Consequently, to connect them effectively to electrical power networks, appropriate and controllable converter equipment is employed. Ideally, a boost converter should have an infinite voltage gain; however, practical limitations such as conduction losses, switch and diode voltage drops hinder achieving this ideal. In practice, a typical setup aims to generate output voltages around 400 V, with input voltage levels ranging from 18 V to 50 V [1, 2, 3, 4, 5]. The performance of power devices in stepping up the voltage is constrained by parasitic capacitance and inductance, conduction losses resulting from resistors, and diode voltage sag. Additionally, the utilization of such a high step-up ratio introduces challenges related to reverse recovery issues and magnetic saturation in the power switch, especially during high-duty cycle operation [6, 7, 8].

The cascading boost converter topology offers the advantage of achieving higher voltage gain without the need for a maximum duty cycle, unlike the conventional boost converter. However, it is important to note that the switches in this topology are subjected to intense voltage and current stress. Another approach to increase voltage gain is through the use of switched inductors and capacitors [9, 10]. Switched converter topologies exhibit double the voltage gain compared to typical step-up converters, but the use of semiconductors leads to higher voltage stress. To address these challenges and enhance voltage gain while minimizing stress on the switches, the voltage lift approach is employed [11, 12]. In scenarios where the conversion ratio is high, a larger number of diodes and capacitors are employed. Limited topologies such as linked inductors and flyback converters utilize the turns ratio and duty cycle to regulate the converter's voltage gain. By achieving the required boost ratio at a medium duty cycle, overall efficiency is improved. Leakage inductance in methodologies like the flyback converter can result in energy dissipation, leading to increased losses. These issues can be mitigated by incorporating passive clamp circuits or active clamp circuits. Switched capacitor converters offer an alternative for boosting without the need for magnetic components [13, 14, 15]. Extensive literature exists on the design of high-gain, high-efficiency boost converters [16, 17, 18, 19, 20, 21]. Topologies employing transformers can achieve high voltage gains by varying the turns ratio of the transformer. Transformers also provide isolation between the input and output sides. Transformer-less topologies compete in terms of cost, weight, and design simplicity [19].

According to Ref. [15], boost converters with hard switching and switched capacitors exhibit a low efficiency of less than 75%. However, the efficiency of switched capacitors can be improved by

incorporating a resonance inductor [22, 23, 24, 25, 26, 27]. Converters with inductors have the ability to adjust their duty cycle for a wide range of boosting, although the compared converter has a somewhat limited boosting range. To address these limitations, this paper introduces a novel ultra-voltage gain boost converter that offers improved performance. The proposed converter, which incorporates a switched inductor circuit, enables high voltage gains and higher output voltages even for low duty ratio values. Therefore, it is well-suited for applications in electric vehicle systems, with a 20V fuel cell output serving as the converter's input voltage. For instance, at a low duty ratio value of D=0.5, the converter can provide output voltages in the range of 50-120V. The proposed ultra-gain boost converter offers several advantages, including enhanced efficiency, reduced voltage stress on active components, and high step capacity.

The paper is organized as follows: Section 2 provides an overview of fuel cells, Section 3 discusses the modeling of fuel cells, Section 4 focuses on fuel cell-based EV systems, Section 5 presents the operation and design analysis of the proposed ultra-gain boost converter and the showcases simulated waveforms, Section 6 presents the results, and finally, Section 7 concludes the paper.

2. Fuel Cell

Since a fuel cell harnesses the chemical energy of hydrogen to produce power, it serves as the input for the proposed converter. Fuel cells offer several advantages over older combustion-based technologies. They operate with higher efficiencies, typically exceeding 60%. Among various fuel cell types, hydrogen fuel cells are particularly popular due to their minimal emissions, generating only water, producing negligible heat, and emitting low levels of pollutants (see Figure 2). Unlike batteries, fuel cells do not suffer from self-discharge and do not require recharging. As long as the fuel and oxygen inputs are available, fuel cells can continuously generate electricity. A typical fuel cell consists of an electrolyte sandwiched between a cathode and an anode. The cathode receives air, while the anode receives fuel such as hydrogen. In a hydrogen fuel cell, a catalyst at the anode facilitates the breakdown of hydrogen molecules into protons and electrons, which then move in opposite directions toward the cathode. The movement of electrons through an external circuit generates electric current. At the cathode, protons combine with oxygen and electrons to produce heat and water as byproducts.

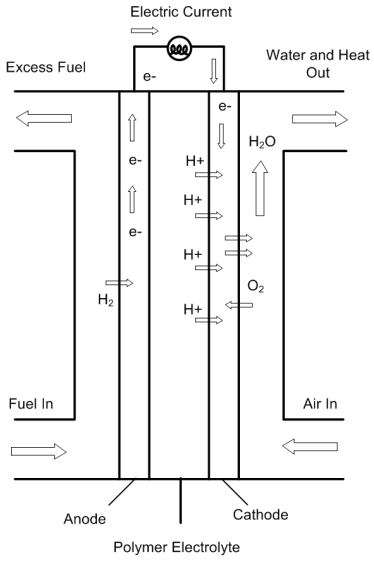

Figure 2. Basic hydrogen fuel-cell.

3. Fuel-cell modelling

The transformation of hydrogen-based chemical energy into electrical energy occurs through the utilization of fuel cells, which are electrochemical devices. Unlike thermal or electromechanical mechanisms, fuel cells facilitate the conversion of oxygen and hydrogen into water and power. When subjected to an electric field, the anode and cathode of the fuel cell undergo specific processes. The movement of ions across the electrodes takes place once equilibrium is established. The fundamental chemical reaction of the Proton Exchange Membrane Fuel Cell (PEMFC) involves oxidation and reduction reactions occurring at the anode and cathode, respectively. At the anode, hydrogen undergoes oxidation to generate protons and electrons, while at the cathode, water is produced through the combination of two protons and two electrons. The overall chemical reaction can be represented as

$$H_2 + \frac{1}{2}O_2 \rightarrow 2H_2O + \text{electrical energy} + \text{heat energy} \tag{1}$$

The voltage generated from the fuel cell is given by

$$V_{\text{FC}} = E_{\text{nernst}} - V_{\text{act}} - V_{\text{ohmic}} - V_{\text{con}}, \tag{2}$$

where V_{act} is used for modeling the activation losses and is given by

$$V_{act} = A \ln\left(\frac{i_{FC} + i_n}{i_0}\right), \tag{3}$$

the voltage drop due to Ohmic losses is given as

$$V_{\text{ohmic}} = R_m \left(i_{FC} + i_n\right), \tag{4}$$

and the concentrations losses are expressed as

$$V_{\text{con}} = -B \ln\left(1 - \frac{i_{\text{FC}} + i_n}{i_1}\right). \tag{5}$$

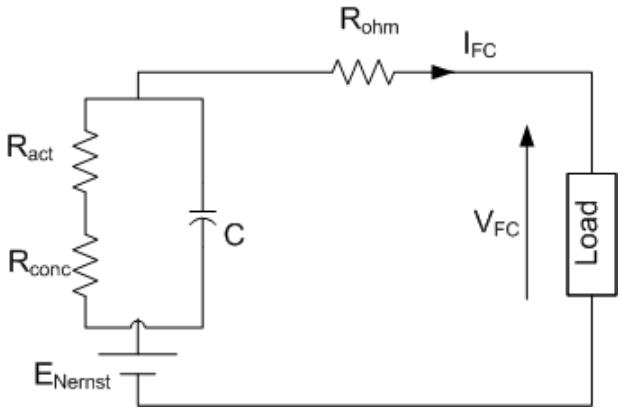

Figure 3. Electrical equivalent circuit.

Figure 3 depicts the electrical equivalent circuit employed for simulating the fuel cell. In comparison to internal combustion engines, fuel cells exhibit significantly reduced or even zero emissions, making them

highly desirable resources for distributed generation systems. When starting a vehicle rapidly, batteries are typically connected in parallel or series with the fuel cells. The fuel cell stack produces a low DC voltage at its output. To obtain higher DC voltages, either additional fuel cells need to be added to the stack or a step-up converter must be employed. In this configuration, instead of using a greater number of fuel cells, a basic boost converter is cascaded with a switched inductor circuit.

4. Fuel-cell based EV system

DC-DC converters typically facilitate power transfer in a unidirectional manner, from the input to the output. However, it is possible to configure DC-DC converters to be bidirectional. Bidirectional topologies are particularly advantageous for applications that require regenerative braking, as they enable power transfer in both directions. By adjusting the duty ratio, the power flow from the input to the output can be controlled. This capability is commonly used to maintain constant power or regulate parameters such as input current, output voltage, and current. Converters incorporating transformers provide isolation between the input and output, although they come with drawbacks such as increased complexity, higher cost, and heavier weight. In the proposed system, the switched inductor circuit serves as the boosting element of the converter. These components are affordable, lightweight, and compact, yet capable of raising the voltage to higher levels. The output of the fundamental boost converter serves as the input to the switched inductor circuit, which further increases the voltage level and delivers a suitable voltage at the output side. The output voltage is then fed to the traction motor through the controller, as depicted in Figure 4. The controller is responsible for regulating the speed and torque of the traction motor, which, in turn, propels the car's wheels through the transmission system.

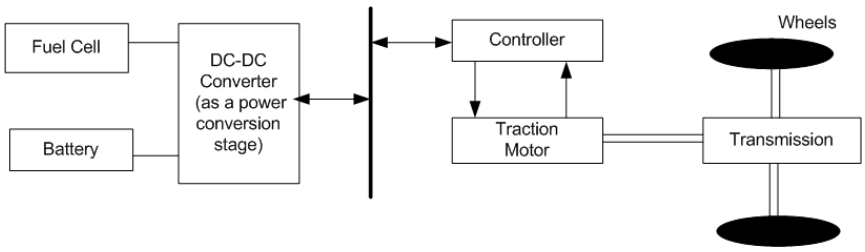

Figure 4. Basic block diagram of fuel cell fed electric vehicle.

5. Proposed Ultra voltage gain Boost converter

The proposed converter's circuit configuration is depicted in Figure 5. It consists of three main elements: the basic boost converter, the switched inductor circuit, and the output filter capacitor. The configuration incorporates three switches, two capacitors, three inductors, and two diodes. The fundamental boost converter circuit is cascaded with the switched inductor circuit, while the output filter capacitor is connected at the output to reduce voltage ripple. In this context, the load represented by the symbol "R" represents a traction motor that drives the wheels of an electric vehicle.

The three switches in the circuit are synchronized to turn ON and OFF simultaneously, while the diodes complement the operation of the switches. When the switches are open, the inductor current follows a clear path. The inductors store energy when the switches are in the ON position and release this energy to the output load when the switches are in the OFF position.

The converter operates in continuous conduction mode (CCM), where the inductor current flows continuously from one end to the other and never reaches zero. Consequently, the inductor partially discharges before each switching cycle. Ideal parameters are assumed for ease of analysis, and a small-ripple

factor is employed in the subsequent analysis. The waveforms corresponding to the proposed converter are illustrated in Figure 6. The following sections discuss two different operating modes in detail.

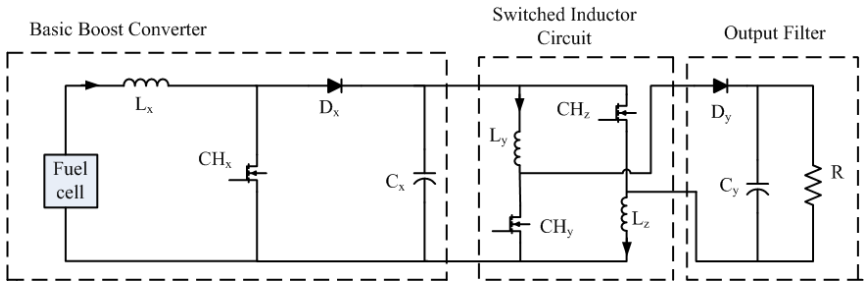

Figure 5. The proposed configuration.

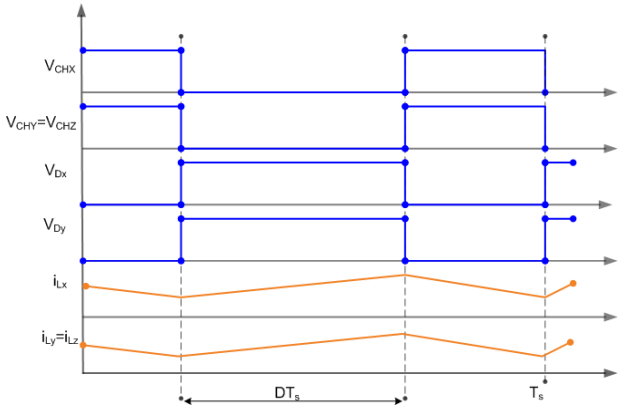

Figure 6. The converter's optimal key waveforms.

5.1. Mode-1

In mode-1, all three switches are turned on simultaneously. The configuration of mode-1 is illustrated in Figure 7. Diodes D_X and D_Y are reverse biased and function in this mode. During this mode, the input DC source charges inductor L_X, while capacitor C_X charges inductors L_Y and L_Z. The energy is released by the two capacitors, C_X and C_Y. While capacitor C_Y releases its energy to the load side, input capacitor C_X releases its energy to inductors L_Y and L_Z. In mode-1, inductors L_Y and L_Z charge simultaneously. The characteristic equations for this mode of operation are depicted in Figure 7.

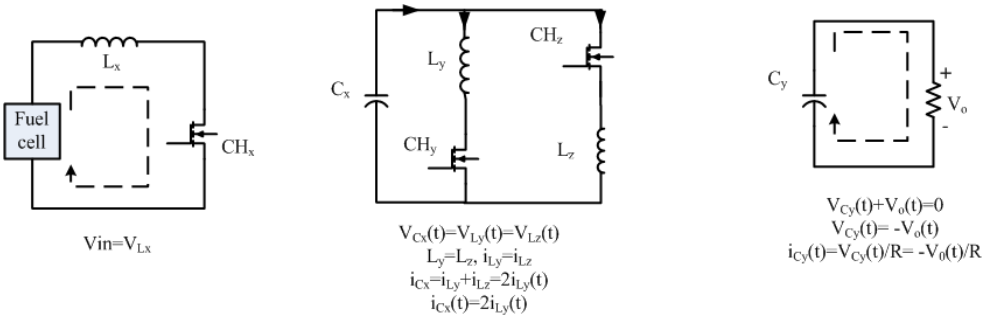

Figure 7. The configurations of mode 1.

5.2. Mode-2

During mode-2, all three switches are simultaneously turned off. The configuration of mode-2 is depicted in Figure 8. In this mode, the energy stored in inductors L_Y and L_Z is discharged to the output capacitor C_Y and the output load, while inductor L_X discharges its energy into capacitor C_X. Two diodes are activated in this mode, serving as freewheeling diodes to provide a continuous path for the inductor currents. In mode-2, inductors L_Y and L_Z are connected in series. The characteristic equations for this mode of operation are presented in Figure 8.

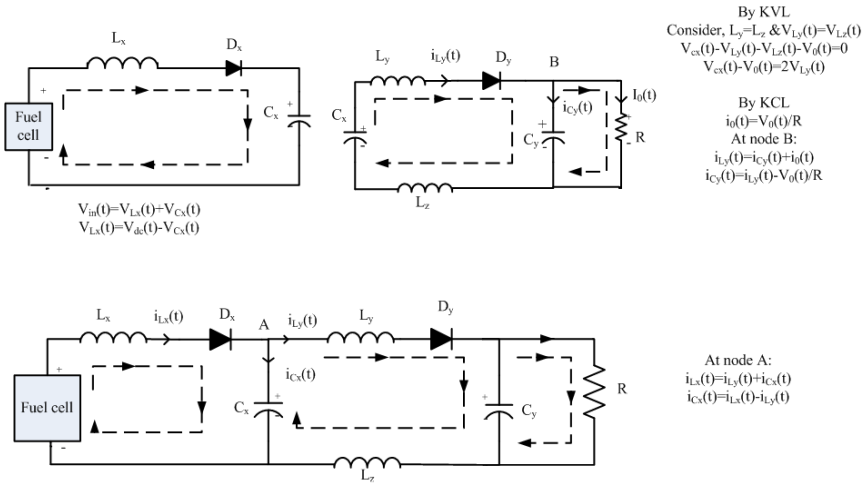

Figure 8. The configurations of mode 2.

From the voltage-second balance principle, the steady state voltage of input capacitor C_X is calculated as follows

$$V_{cx}(t) = \frac{V_{in}(t)(T_{ON} + T_{OFF})}{T_{OFF}}, \tag{6}$$

where T_{ON} and T_{OFF} are the periods in turn on and turn off of the switches, respectively. Thus, the average voltage of the capacitor C_X can be calculated by

$$V_{cx(avg)} = V_{in}\left(\frac{1}{1-D}\right), \tag{7}$$

with

$$D = \frac{T_{ON}}{T_{\text{total}}}, \tag{8}$$

where $T_{\text{total}} = T_{\text{ON}} + T_{\text{OFF}}$.

From the loop equations in mode1 and mode 2 configurations,

$$V_{cx(avg)} = V_0\left(\frac{1-D}{1+D}\right) \tag{9}$$

Equation (7) provides the voltage gain of the converter based on the information above.

$$\frac{V_0}{V_{in}} = \frac{1+D}{(1-D)^2} \tag{10}$$

Tables 1 and 2 show, respectively, the voltage and current stresses of each component, which are stressed at a lower voltage than that of the output voltage. This aids in our decision-making process when selecting low-rated devices, increasing the overall effectiveness of the system. The benefit of this design is that each component has a voltage stress that is lower than the output voltage, and the overall effectiveness of the system is increased because it allows us to choose devices that have low ratings.

Switching Device	Voltage Stress at Peak
CH_x	$V_o(1-D)/(1+D)$
CH_y	$V_o/(1+D)$
CH_z	$V_o/(1+D)$
D_X	$V_o(1-D)/(1+D)$
D_y	$2V_o/(1+D)$

Table 1. The switching voltage stresses of the devices.

Switching Device	RMS Current Stress
CH_x	$I_{i_n}\sqrt{(D)}$
CH_y	$(1-D)\sqrt{D}I_{i_n}/2$
CH_z	$(1-D)\sqrt{D}I_{i_n}/2$
Free-Switch Diodes	**Average Current Stress**
D_X	$I_{i_n}(1-D)$
D_y	$(1-D)^2 I_{i_n}/2$

Table 2. The switching current stresses of the devices.

5.3. Inductor L_x design

The current in the inductor L_x is shown in Figure 9. I_1 stands for the inductor L_x average current value, and Δi_{L_x} is the difference between the peak and average currents. The ripple of inductor L_x is given for the first interval of the switching cycle as

$$L_x = \left(\frac{V_{in}}{2\Delta i_{Lx}}\right) DT_s, \tag{11}$$

where V_{in} is the input voltage, D is the duty cycle, and T_s is the sample time.

5.4. Inductor L_y and L_z

Similar to the current through the L_z, Figure 10 represents the inductor L_y current waveform. It is stated as the difference between the average current and peak current of the inductor, and it stands in for the average value of the L_y current. When the first interval of the switching cycle is taken into account, the ripple in the inductors L_y and L_z are estimated as,

$$L_y = L_z = \left(\frac{V_{in}}{2\Delta i_{Ly}}\right)\left(\frac{DT_s}{1-D}\right). \tag{12}$$

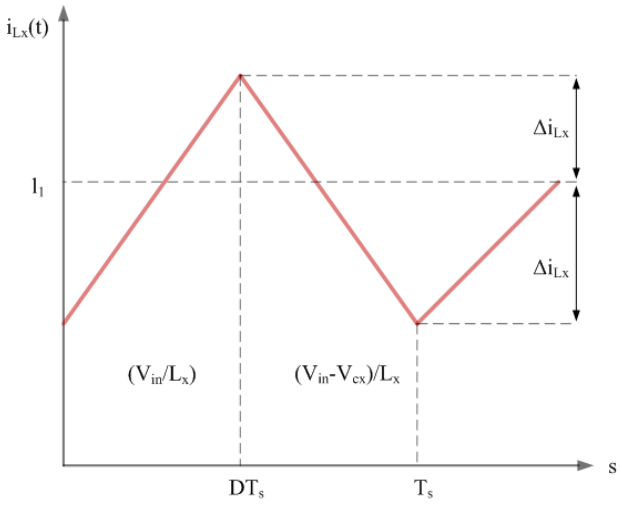

Figure 9. The inductor L_x current

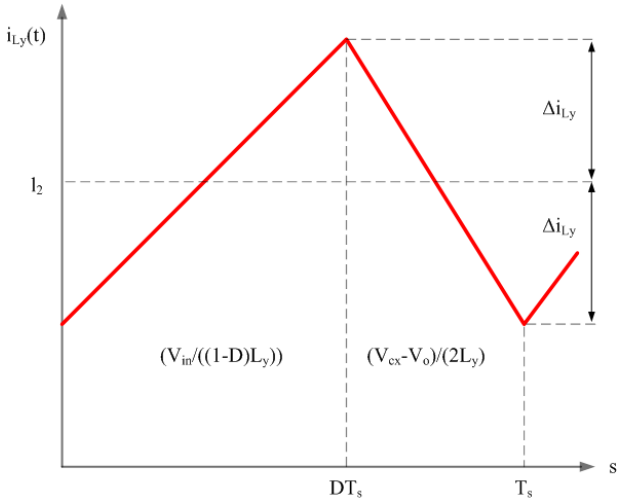

Figure 10. The currents in the inductors L_y and L_z.

5.5. Capacitor C_x design

The current of the capacitor C_x is the same as that of inductor L_x, without the dc components (see Figure 10). Figure 11 shows the capacitor voltage as it approaches its maximum and minimum limits at the two zero crossing points of its current waveforms. The greatest ripple of the capacitor C_x voltage and total charge q have the following relationship

$$q = C_x(2\Delta V_{cx}), \tag{13}$$

where ΔV_{cx} is the difference between the average and the maximum capacitor voltage values.

The capacitor symmetry determines the current waveform, and the charge q value is determined by embedding the shaded portion of the C_x current as

$$q = \frac{1}{2}\Delta i_{Lx}\frac{T_s}{2}. \tag{14}$$

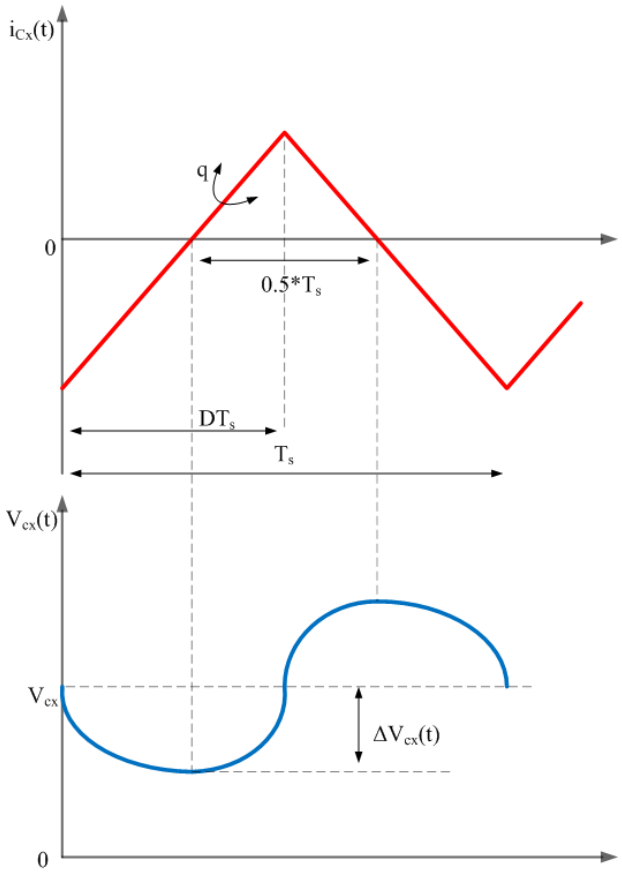

Figure 11. Current and voltage in the capacitor C_x.

Equation (13) is replaced in Equation (14), and the voltage ripple peak amplitude solution is obtained as,

$$\Delta v_x = \frac{\Delta i_{Lx} T_s}{8C_x}, \tag{15}$$

and the capacitor value is calculates as,

$$C_x = \frac{\Delta i_{Lx} T_s}{8\Delta V_{cx}}. \tag{16}$$

Note that the capacitor value is influenced by the sampling interval T_s, the permitted ripple on the capacitor C_x, and the current ripple of the inductor i_{Lx}.

5.6. Output Capacitor C_y

The quantity of ripple allowed in the capacitor voltage C_y limits the output voltage ripple of the converter. To keep the converter output voltage ripple within the permitted range, capacitor C_y must be constructed. Figure 12 shows the capacitor C_y voltage along with the mean capacitor voltage V_o and the discrepancy between the median wage and peak capacitor voltages V_o. By taking into account the first switching cycle duration, the ripple of capacitor C_y is determined as,

$$\Delta C_y = \left(\frac{V_o}{2\Delta V_o}\right) DT_s. \tag{17}$$

Component	Description	Specification
V_{in}	Input voltage	20V
V_o	Output voltage	60V
L_x	Inductor	11.33µH
L_y, L_z	Inductors	20.83µH
C_x	Input Capacitor	20.83µF
C_y	Output Capacitor	34µF
R_o	Resistor	1.44Ω
$M(D) = V_o/V_{in}$	Gain	3
D	Duty Ratio	0.34
f_s	Switching Frequency	60000Hz
P_o	Rated Output Power	2500W

Table 3. Simulation component values.

Note that the capacitor C_y value is influenced by the output voltage V_o, duty cycle D, sampling time T_s, and capacitor voltage ripple V_o.

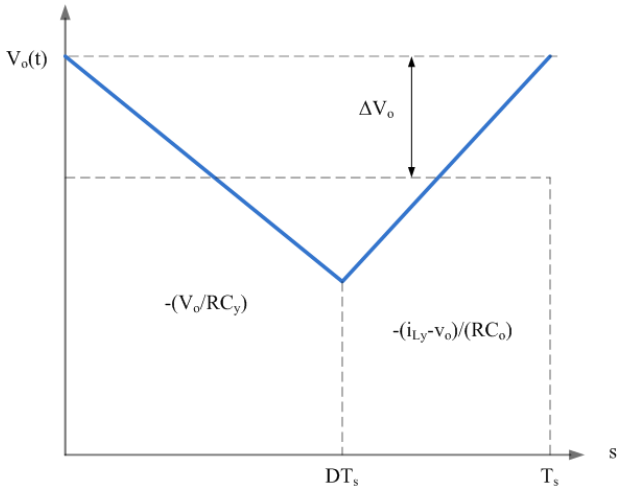

Figure 12. Output voltage in The capacitor C_y.

6. Results

To validate the operational characteristics and assess the performance of the proposed converter, a simulation using MATLAB software was conducted. The simulation parameters required to replicate the proposed converter are provided in Table 3. For the simulation, an input voltage of 20V was considered, while the converter was designed to deliver an output power of 2.5KW. To achieve compact converter dimensions, higher switching frequencies (f_s) were recommended. In this design, a frequency of 60 kHz was chosen. The converter configuration consists of three inductors, two capacitors, and five energy elements. The values of the energy components were carefully determined to ensure appropriate current and voltage ripples on the inductors and capacitors, respectively.

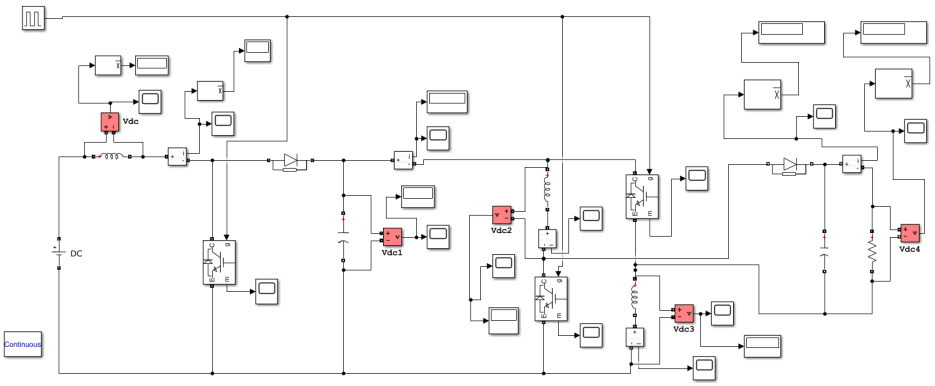

Figure 13. Simulation diagram of the proposed converter.

Figure 13 shows the Matlab simulation diagram used to assess the viability and validity of the suggested ultra-voltage gain boost converter. The duty ratio was set at 0.34, the input side voltage is 20V, and the evaluated output side voltage across the converter is approximately 60V. The waveforms of the switch voltages are shown in Figures 14 and 15. While switches CH_x and CH_y experience different voltage stresses, CH_y and CH_z experience similar voltage stresses. Compared to switch voltage stresses across CH_y and CH_z the switch voltage stress across CH_x has a lower value.

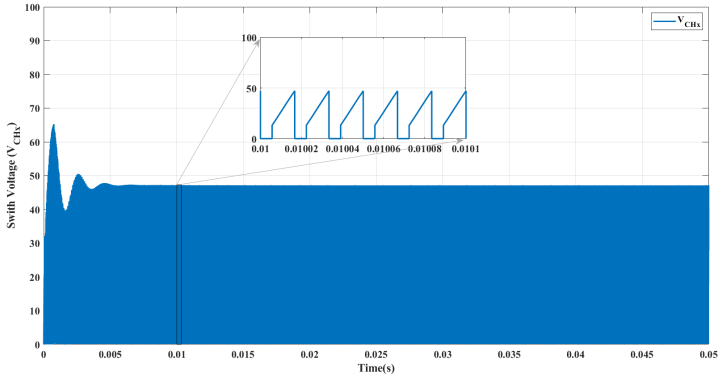

Figure 14. switch CH_x voltage stress waveform.

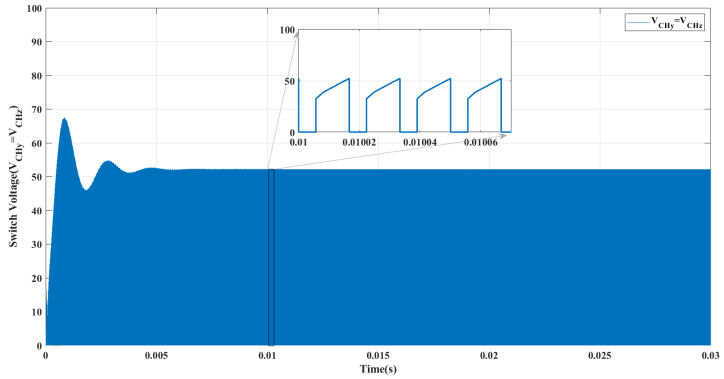

Figure 15. switch CH_y and CH_z voltage stress waveforms.

Figure 16 shows the simulation results of voltage stress waveform across capacitor CH_x of the designed converter. The charging and discharging of capacitor CH_x is observed in the simulated waveform and it is deduced that theoretical analysis of the ripple value is exactly similar to the value of ripple content obtained through simulation. Figure 17 shows the simulation results of the input current waveform at Duty ratio D=0.34.

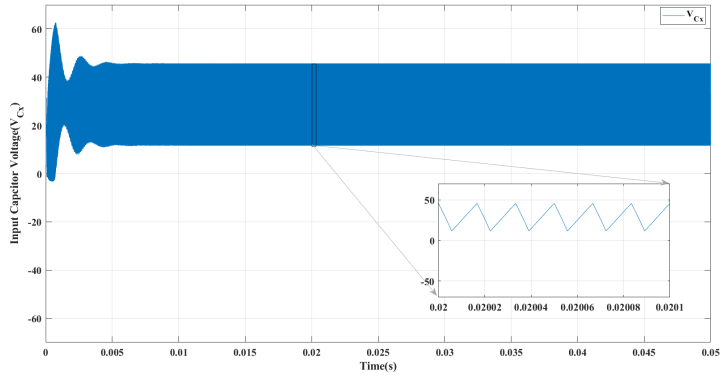

Figure 16. Input capacitor CH_x voltage stress waveform.

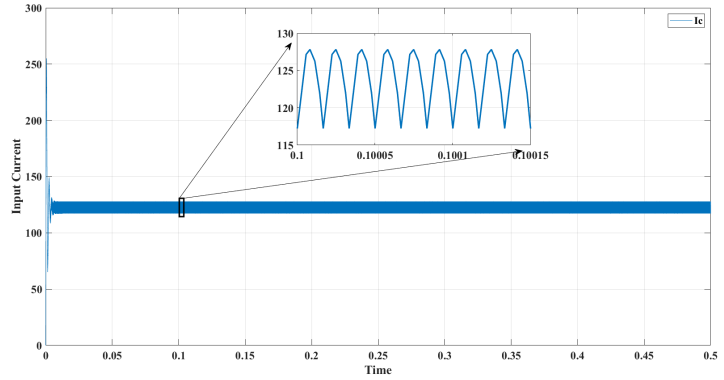

Figure 17. Input current waveform.

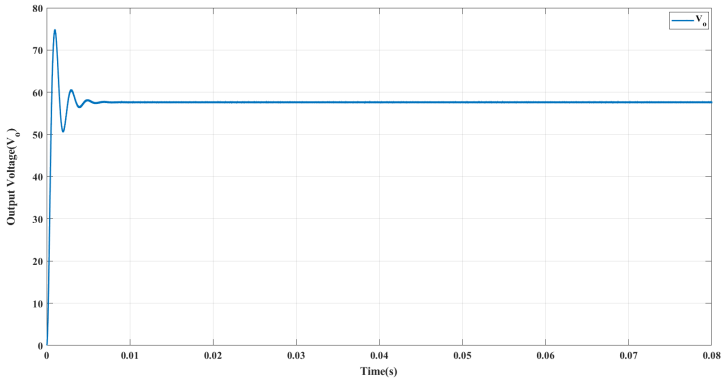

Figure 18. Output voltage waveform.

Figure 18 shows the suggested predicted output voltage waveform of the model. When the input voltage is 20V and the duty ratio is set to 0.34, the theoretical output voltage is roughly 60V. The simulation produced an output voltage value of 60V. The output voltage derived through theoretical analysis is equivalent to it.

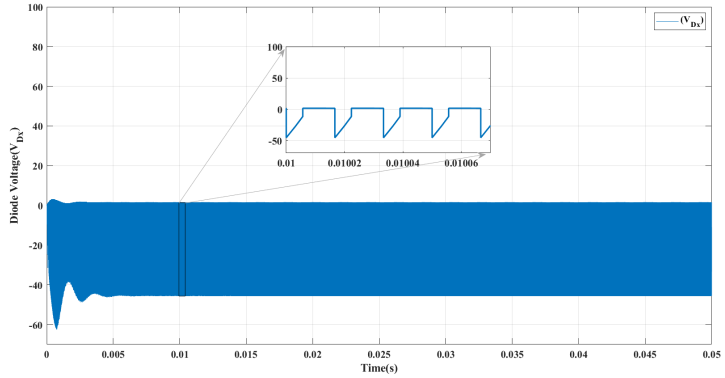

Figure 19. Diode D_X voltage stress waveforms.

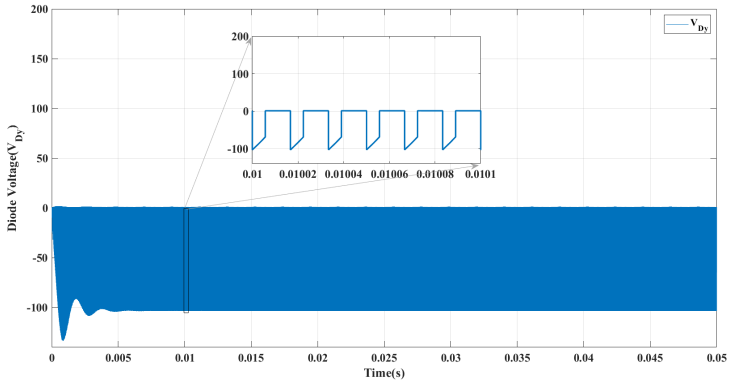

Figure 20. Diode D_Y voltage stress waveforms.

Figures 19 and 20 show the simulated Diode voltage stress waveforms of the suggested converter. Diode voltage stresses are lower in value and are shown with negative values.

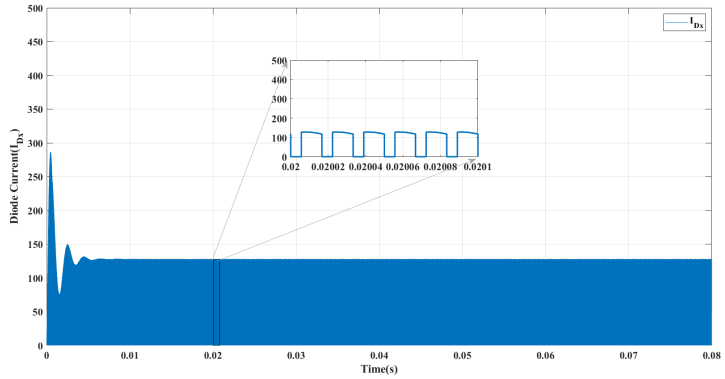

Figure 21. Diode D_X current stress waveform

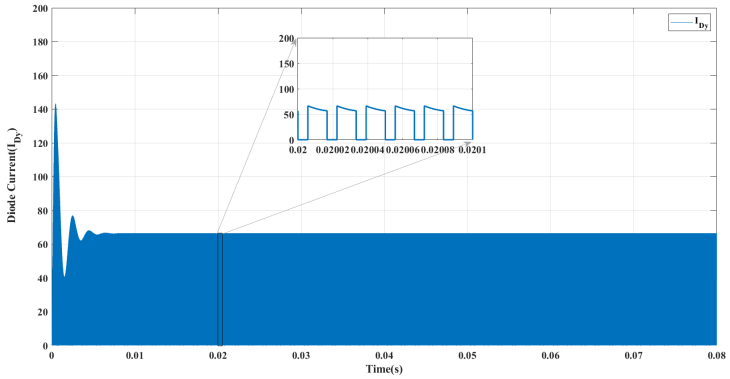

Figure 22. Diode D_Y current stress waveform

Figures 21 and 22 show the simulated current stress waveforms of the suggested converter for the Diode D_x and D_y, respectively. For proper demonstration, a steady-state segment with few complete cycles is exhibited in the figures. Diode current stresses are lower in value.

Analysis is done on the converter's performance in terms of output power, output voltage, output current, and efficiency. The table presents the simulated values of different parameters for various duty ratios. From performance Table 4, it is clear that for varied duty ratios, the suggested converter maintains higher efficiency. As the value of the duty ratio increases, losses increase, and efficiency slightly drops.

Table 5 gives the comparison between theoretical and simulated values of switch voltage stresses for various duty ratios. Upto 50% duty ratio, the theoretical values are almost equal to the simulated values. Beyond 50% duty ratio, the switch voltage stresses increase exponentially.

To understand clearly the characteristics of the designed converter, the graphs of various parameters concerning duty ratio are plotted (Figures 23- 27) and they clearly show how the specific parameter changes with respect to changes in duty ratios.

D	V_o	I_o	P_o	P_{i_n}	$\%\eta$
10	25.90	18.03	468.23	489.6	95.60
15	30.38	21.09	640.71	671.0	95.40
20	35.66	24.77	883.29	928.4	95.10
25	42.11	29.25	1231.71	1301.4	94.60
30	49.97	34.70	1733.90	1847.6	93.80
34	57.56	34.97	2300.67	2476.0	92.91
35	59.67	41.44	2472.70	2668.0	92.60
40	71.59	49.72	3559.40	3912.0	90.90
45	82.26	57.12	4698.60	5276.0	89.05
50	89.24	61.98	5531.00	6340.0	87.70
55	97.34	67.60	6580.10	7752.0	84.80
60	106.90	74.20	7931.90	9692.0	81.80

Table 4. Performance of Proposed converter.

D	$V_{CH_X}(T)$	$V_{CH_X}(S)$	$V_{CH_y}(T)$	$V_{CH_y}(S)$	$V_{CH_z}(T)$	$V_{CH_z}(S)$
10	22.22	22.28	24.69	24.18	24.69	24.18
15	23.52	23.69	27.68	26.82	27.68	26.82
20	25.00	24.90	31.25	30.38	31.25	30.38
25	26.66	26.60	35.55	34.80	35.55	34.80
30	28.57	27.20	40.81	39.80	40.81	39.80
34	30.30	30.35	45.91	44.10	45.91	44.10
35	30.76	32.50	47.33	45.40	47.33	45.40
40	33.33	35.50	55.55	53.70	55.55	53.70
45	36.36	40.40	66.11	60.70	66.11	60.70
50	40.00	41.12	80.00	67.42	80.00	67.42
55	44.44	46.00	98.76	70.76	98.76	70.76
60	50.00	54.40	125.00	77.20	125.00	77.20

Table 5. Switch voltage stresses of proposed converter.

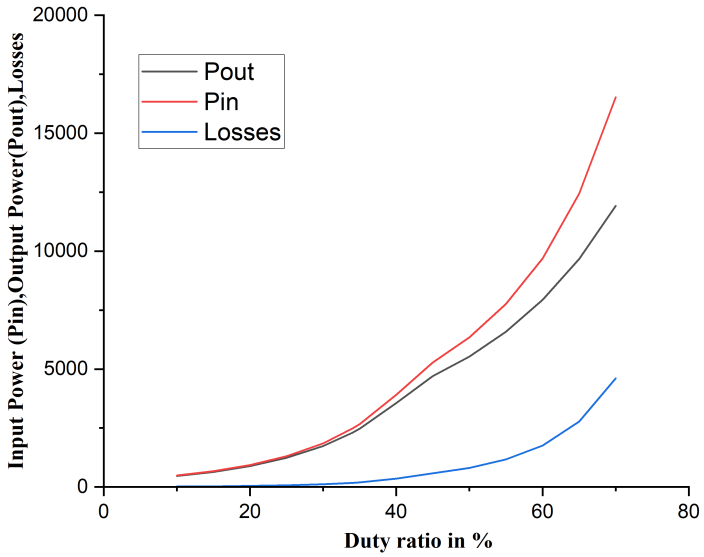

Figure 23. Power vs duty ratio.

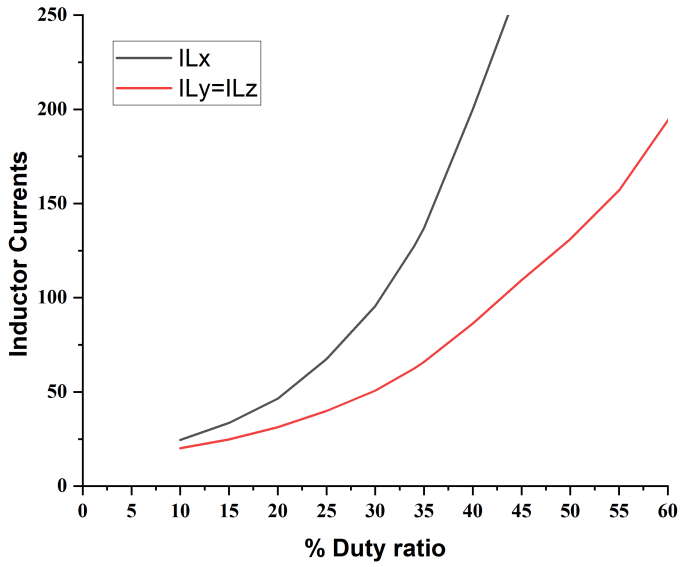

Figure 24. Inductor currents vs duty ratio.

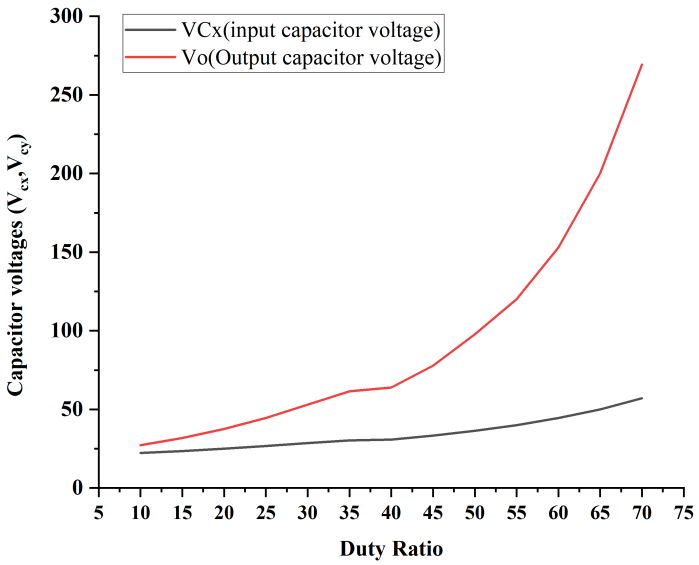

Figure 25. Capacitor voltages vs duty ratio.

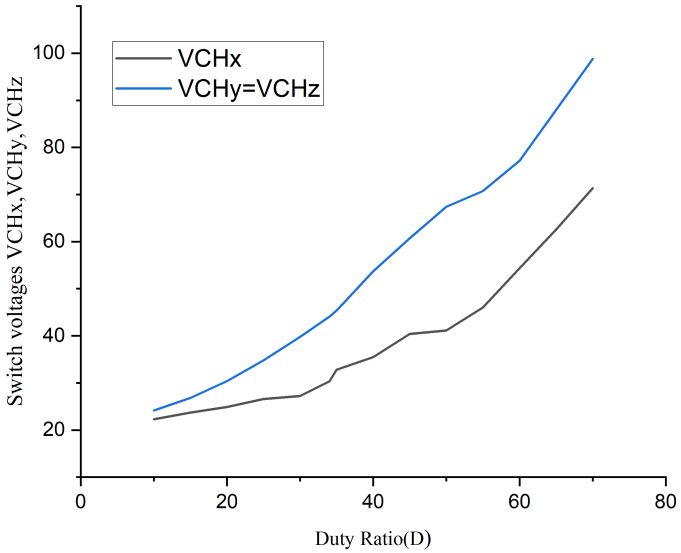

Figure 26. Switch voltages vs duty ratio.

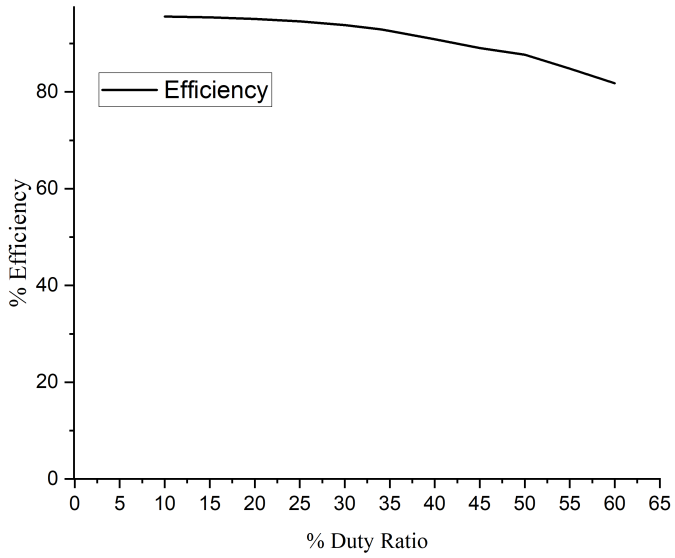

Figure 27. Efficiency vs duty ratio.

Table 6 provides a comparison of the proposed converter with existing topologies in terms of the number of energy elements, switches, diodes, and voltage gain. The graph of voltage gain as a function of the duty ratio for the converters is illustrated in Figures 28 and 29. It can be observed that the suggested converter achieves a significantly higher boost factor compared to other converters at the same duty ratio. The limitations of the conventional boost converter in terms of achieving high voltage gain are evident

from Table 6. On the other hand, the proposed boost converter achieves a high boost factor given by $(1+D)/(1-D)^2$ when compared to the traditional boost converter. The utilization of low-rated energy elements contributes to cost reduction and compactness of the converter.

S.No	Converter	No.of Inductors	No.of Capacitors	No.of Diodes	No.of Power switches	Total No.of Components	Voltage Gain
1	Boost	1	1	1	1	4	$1/(1-D)$
2	SL Boost	2	1	4	1	8	$(1+D)$ / $(1-D)$
3	SC Boost	1	3	1	1	6	$1/(1-D)$
4	Non-isolated bidirectional DC-DC converter [24]	2	3	0	4	9	$1/(1-D)^2$
5	A New High-Gain DC-DC Converter [25]	2	2	2	2	8	$(1+D-D^2)$/ $(1-D)^2$
6	An interleaved boost DC-DC converter [26]	2	3	4	2	11	$2/(1-D)$
7	Non-isolated high step-up DC–DC converters [27]	2	5	4	1	12	$(2+D)$/ $(1-D)$
8	Ultra-voltage gain boost converter	3	2	2	3	10	$(1+D)$/ $(1-D)^2$

Table 6. Comparison values of the proposed converter with different converter topologies.

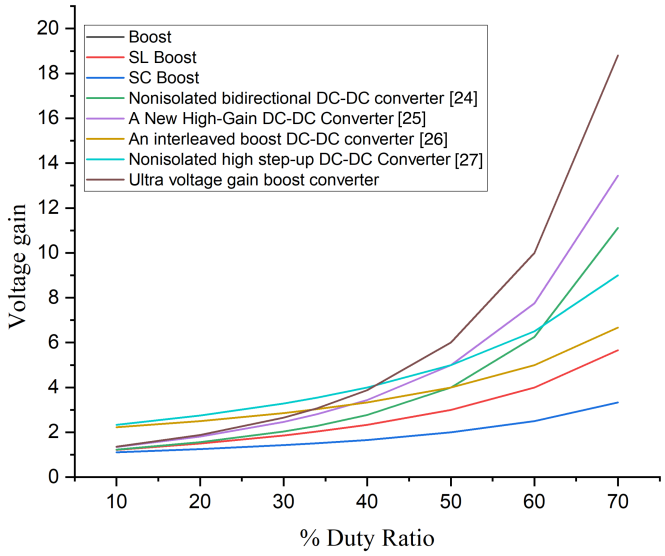

Figure 28. Voltage gain comparison between the suggested converter and different topologies.

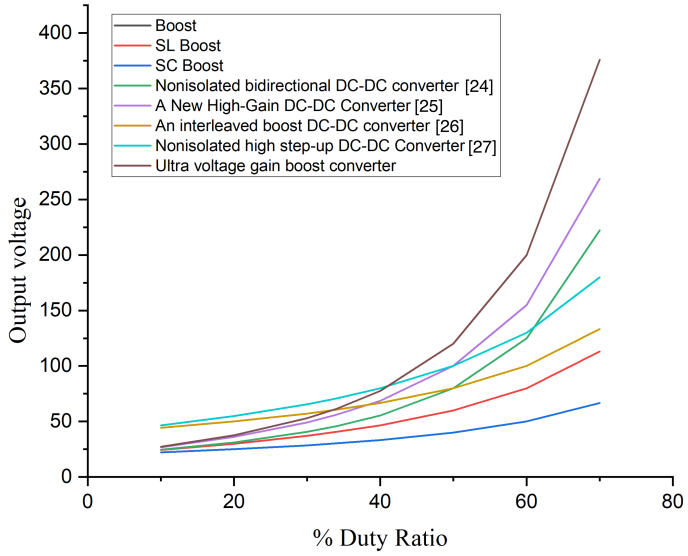

Figure 29. Comparison of the proposed converter's output voltage to that of other topologies.

Figures 28 and 29 present characteristic curves illustrating the voltage gain and output voltage of various converter topologies, enabling an evaluation of the performance level achieved by the proposed converter. The suggested converter demonstrates higher output voltages at lower duty ratios compared to existing topologies. A notable advantage of the proposed converter is its ability to achieve a larger voltage gain

while operating under reduced voltage and current stresses. Moreover, the suggested converter exhibits significantly higher output voltage and voltage gain when compared to alternative topologies.

7. Conclusion

A fuel cell based ultra-voltage gain boost converter for electrical vehicle applications was proposed. Three switches, two diodes, two capacitors, and three inductors make up the designed configuration. The performance of the proposed converter in continuous current mode for steady state condition is analyzed. The proposed boost converter may be seen to deliver considerable voltage gain even at low duty ratios. When compared to the topologies that are currently in use, the suggested converter has reduced voltage and current stresses. Therefore, the efficiency of the proposed converter was high for various duty ratios. The theoretical interpretation was provided to support the experimental findings. The converter that is proposed has characteristics like increased step-up gain voltage, continuous input current, increasing efficiency, and fewer components. Hence, it is suitable for fuel-cell systems and Electric vehicle applications.

Author contributions: Conceptualization: Dr. B. Nagi Reddy; Methodology: Dr. B. Nagi Reddy and G. Vinay Kumar; Investigation: G. Vinay Kumar, and B. Vinay Kumar; Writing: B. Jhansi, and B. Sandeep; Writing – Review and Editing: Dr. B. Nagi Reddy and Dr. K, Sarada; Supervision: Dr. B. Nagi Reddy.

Disclosure statement: The authors declare no conflict of interest.

References

[1] Phani Teja Bankupalli, Subhojit Ghosh, Lalit Kumar, and Susovon Samanta. Fractional order modeling and two loop control of pem fuel cell for voltage regulation considering both source and load perturbations. *International journal of hydrogen energy*, 43(12):6294–6309, 2018.

[2] Ahmad W Al-Dabbagh, Lixuan Lu, and Antonio Mazza. Modelling, simulation and control of a proton exchange membrane fuel cell (pemfc) power system. *International Journal of Hydrogen Energy*, 35(10):5061–5069, 2010.

[3] Sahithi Priya KOSİKA, Manish Patel GADAM, Jagadhishwar BANOTH, Ashok BANOTH, GOUD Srikanth, et al. Analysis of positive output buck-boost topology with extended conversion ratio. *Journal of Energy Systems*, 6(1):62–83, 2022.

[4] Mohammad Zaid, Chang-Hua Lin, Shahrukh Khan, Javed Ahmad, Mohd Tariq, Arshad Mahmood, Adil Sarwar, Basem Alamri, and Ahmad Alahmadi. A family of transformerless quadratic boost high gain dc-dc converters. *Energies*, 14(14):4372, 2021.

[5] Eduardo Augusto Oliveira Barbosa, Márcio Rodrigo Santos de Carvalho, Leonardo Rodrigues Limongi, Marcelo Cabral Cavalcanti, Eduardo José Barbosa, and Gustavo Medeiros de Souza Azevedo. High-gain high-efficiency dc–dc converter with single-core parallel operation switched inductors and rectifier voltage multiplier cell. *Energies*, 14(15):4634, 2021.

[6] Aline VC Pereira, Marcelo C Cavalcanti, Gustavo M Azevedo, Fabrício Bradaschia, Rafael C Neto, and Márcio Rodrigo Santos de Carvalho. A novel single-switch high step-up dc–dc converter with three-winding coupled inductor. *Energies*, 14(19):6288, 2021.

[7] Lucas Carvalho Souza, Douglas Carvalho Morais, Luciano de Souza da Costa e Silva, Falcondes José Mendes de Seixas, and Luis De Oro Arenas. Dc-dc 3ssc-a-based boost converter: Analysis, design, and experimental validation. *Energies*, 14(20):6771, 2021.

[8] Hossein Gholizadeh, Saman A Gorji, Ebrahim Afjei, and Dezso Sera. Design and implementation of a new cuk-based step-up dc–dc converter. *Energies*, 14(21):6975, 2021.

[9] Jian Ai and Mingyao Lin. Ultralarge gain step-up coupled-inductor dc–dc converter with an asymmetric voltage multiplier network for a sustainable energy system. *IEEE Transactions on Power Electronics*, 32(9):6896–6903, 2016.

[10] Yun Zhang, Yongping Gao, Lei Zhou, and Mark Sumner. A switched-capacitor bidirectional dc–dc converter with wide voltage gain range for electric vehicles with hybrid energy sources. *IEEE Transactions on Power Electronics*, 33(11):9459–9469, 2018.

[11] Boris Axelrod, Yefim Berkovich, and Adrian Ioinovici. Switched-capacitor/switched-inductor structures for getting transformerless hybrid dc–dc pwm converters. *IEEE Transactions on Circuits and Systems I: Regular Papers*, 55(2):687–696, 2008.

[12] Chung-Ming Young, Ming-Hui Chen, Tsun-An Chang, Chun-Cho Ko, and Kuo-Kuang Jen. Cascade cockcroft–walton voltage multiplier applied to transformerless high step-up dc–dc converter. *IEEE transactions on industrial electronics*, 60(2):523–537, 2012.

[13] Fernando Lessa Tofoli, Denis de Castro Pereira, Wesley Josias de Paula, and Demercil de Sousa Oliveira Junior. Survey on non-isolated high-voltage step-up dc–dc topologies based on the boost converter. *IET power Electronics*, 8(10):2044–2057, 2015.

[14] Zbigniew Waradzyn, Robert Stala, Andrzej Mondzik, Adam Penczek, Aleksander Skala, and Stanislaw Pirog. Efficiency analysis of mosfet-based air-choke resonant dc–dc step-up switched-capacitor voltage multipliers. *IEEE Transactions on Industrial Electronics*, 64(11):8728–8738, 2017.

[15] Alon Cervera, Michael Evzelman, Mor Mordechai Peretz, and Shmuel Ben-Yaakov. A high-efficiency resonant switched capacitor converter with continuous conversion ratio. *IEEE Transactions on Power Electronics*, 30(3):1373–1382, 2014.

[16] Andrii Chub, Dmitri Vinnikov, Frede Blaabjerg, and Fang Zheng Peng. A review of galvanically isolated impedance-source dc–dc converters. *IEEE Transactions on Power Electronics*, 31(4):2808–2828, 2015.

[17] Omar Abdel-Rahim, Andrii Chub, Andrei Blinov, and Dmitri Vinnikov. New high-gain non-inverting buck-boost converter. *IECON 2021–47th Annual Conference of the IEEE Industrial Electronics Society*, pages 1–6, 2021.

[18] Álvaro Ojeda-Rodríguez, Pablo González-Vizuete, Joaquín Bernal-Méndez, and María A Martín-Prats. A survey on bidirectional dc/dc power converter topologies for the future hybrid and all electric aircrafts. *Energies*, 13(18):4883, 2020.

[19] Alencar Franco de Souza, Fernando Lessa Tofoli, and Enio Roberto Ribeiro. Switched capacitor dc-dc converters: A survey on the main topologies, design characteristics, and applications. *Energies*, 14(8):2231, 2021.

[20] Mojtaba Forouzesh, Yam P Siwakoti, Saman A Gorji, Frede Blaabjerg, and Brad Lehman. Step-up dc–dc converters: a comprehensive review of voltage-boosting techniques, topologies, and applications. *IEEE transactions on power electronics*, 32(12):9143–9178, 2017.

[21] António Manuel Santos Spencer Andrade and Mário Lùcio da Silva Martins. Quadratic-boost with stacked zeta converter for high voltage gain applications. *IEEE Journal of Emerging and Selected Topics in Power Electronics*, 5(4):1787–1796, 2017.

[22] Robert Stala, Zbigniew Waradzyn, Andrzej Mondzik, Adam Penczek, and Aleksander Skała. Dc–dc high step-up converter with low count of switches based on resonant switched-capacitor topology. *2019 21st European Conference on Power Electronics and Applications (EPE'19 ECCE Europe)*, pages P–1, 2019.

[23] Masahito Shoyama, Toshiyuki Naka, and Tamotsu Ninomiya. Resonant switched capacitor converter with high efficiency. *2004 IEEE 35th Annual Power Electronics Specialists Conference (IEEE Cat. No. 04CH37551)*, 5:3780–3786, 2004.

[24] Hossein Ardi, Ali Ajami, Faezeh Kardan, and Shahla Nikpour Avilagh. Analysis and implementation of a nonisolated bidirectional dc–dc converter with high voltage gain. *IEEE Transactions on Industrial Electronics*, 63(8):4878–4888, 2016.

[25] Javed Ahmad, Mohammad Zaid, Adil Sarwar, Chang-Hua Lin, Mohammed Asim, Raj Kumar Yadav, Mohd Tariq, Kuntal Satpathi, and Basem Alamri. A new high-gain dc-dc converter with continuous input current for dc microgrid applications. *Energies*, 14(9):2629, 2021.

[26] Roger Gules, L Lopes Pfitscher, and L Claudio Franco. An interleaved boost dc-dc converter with large conversion ratio. *2003 IEEE International Symposium on Industrial Electronics (Cat. No. 03TH8692)*, 1:411–416, 2003.

[27] Gang Wu, Xinbo Ruan, and Zhihong Ye. Nonisolated high step-up dc–dc converters adopting switched-capacitor cell. *IEEE Transactions on Industrial Electronics*, 62(1):383–393, 2014.